Multimodal Unsupervised Spatio-Temporal Interpolation of Satellite Ocean Altimetry Maps

4 authors:

Théo Archambault
Sorbonne Université
9 PUBLICATIONS **18** CITATIONS

SEE PROFILE

Arthur Filoche
University of Western Australia
12 PUBLICATIONS **36** CITATIONS

SEE PROFILE

Anastase Alexandre Charantonis
École Nationale Supérieure d'Informatique pour l'Industrie et l'entreprise
41 PUBLICATIONS **244** CITATIONS

SEE PROFILE

Dominique Béréziat
Sorbonne Université
84 PUBLICATIONS **392** CITATIONS

SEE PROFILE

Multimodal Unsupervised Spatio-Temporal Interpolation of satellite ocean altimetry maps

Théo Archambault[1*], Arthur Filoche[1], Anastase Charantonnis[2,3] and Dominique Béréziat[2]

[1]*LIP6, Sorbonne University, 4 place Jussieu, Paris, France*

[2]*LOCEAN, Sorbonne University, 4 place Jussieu, Paris, France*

[3]*ENSIEE, Evry, France*

Corresponding author: theo.archambault@lip6.fr

Abstract: Satellite remote sensing is a key technique to understand Ocean dynamics. Due to measurement difficulties, various ill-posed image inverse problems occur, and among them, gridding satellite Ocean altimetry maps is a challenging interpolation of sparse along-tracks data. In this work, we show that it is possible to take advantage of better-resolved physical data to enhance Sea Surface Height (SSH) gridding using only partial data acquired via satellites. For instance, the Sea Surface Temperature (SST) is easier to measure through satellite and has an underlying physical link with altimetry. We train a deep neural network to estimate a time series of SSH using a time series of SST in an unsupervised way. We compare to state-of-the-art methods and report a 13% RMSE decrease compared to the operational altimetry algorithm.

1 INTRODUCTION

Due to their massive heat storage capacity, the oceans play a crucial role in climate regulation. Understanding their dynamics is essential in many applications such as oceanography, meteorology, navigation, and others. This has motivated the establishment of numerous satellite-based ocean-monitoring missions. Among them, satellite altimetry is used to retrieve the Sea Surface Height (SSH), a variable conditioning ocean circulation. The recovery of the global SSH from satellite imaging constitutes a challenging Spatio-Temporal interpolation image inverse problem. SSH is currently measured by various nadir-pointing altimeters, meaning that they can only take measurements vertically, along their very sparse ground tracks. The gridded SSH image is reconstructed through the Data Unification and Altimeter Combination System (DUACS) (Taburet et al., 2019). This algorithm performs a linear optimal interpolation with a covariance matrix estimated on 25 years of observations. However, it has been shown that this product misses mesoscales dynamics and eddies (Amores et al., 2018; Stegner et al., 2021). To enhance SSH recovery, a new altimeter called SWOT (Surface Water and Ocean Topography) will be launched in the close future. It will provide two 60-km-wide swaths separated 20-km gap instead of nadir observations. Even with this additional coverage, the dynamics of small-scale structures will still not be observable due to the low measurement time frequency (Gaultier et al., 2016).

In the past years, various mapping methods have been proposed to improve DUACS optimal interpolation including model-based approaches (Le Guillou et al., 2020; Ballarotta et al., 2020; Ardhuin et al., 2020) and data-driven approaches (Fablet et al., 2021).

Deep neural networks, and especially convolutional neural networks, have proven their ability to solve ill-posed image inverse problems (Jam et al., 2021; McCann et al., 2017; Ongie et al., 2020; Qin et al., 2021; Wang et al., 2021; Fablet et al., 2021). Among them, (Fablet et al., 2021) introduced a deep learning network that outperforms model-driven methods demonstrating the interest in using trainable models. Furthermore, the flexibility of deep learning-based methods allows us to use information from other sources than only the SSH, by learning the underlying physical link between multimodal observations. For instance, the Sea Surface Temperature (SST) can be retrieved at a much better resolution (1.1 to 4.4 km) than the SSH from the AVHRR instruments (Emery et al., 1989). These two variables
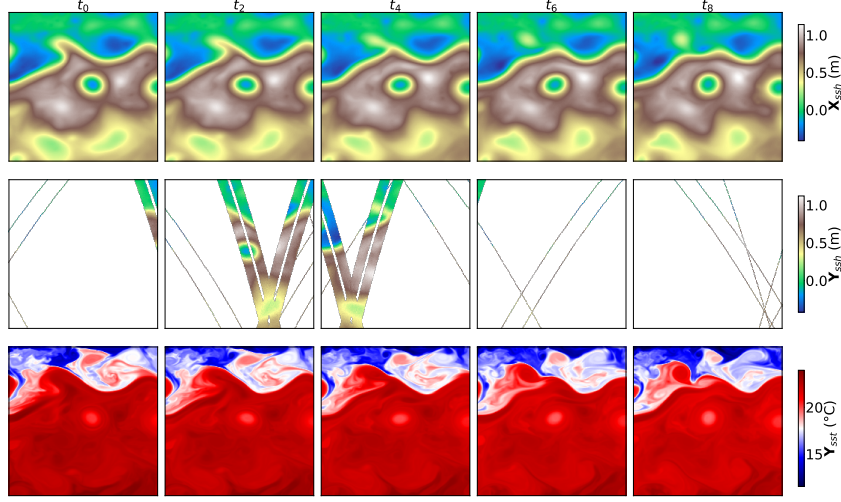
Figure 1: NATL60 output data in a 10-day time window (the time step is 2-day). The first row is the ground truth SSH, and the second is the twin experiment on SSH along tracks. The wide satellite tracks simulate SWOT satellites whereas the fine tracks simulate nadir observations. The last row is the modeled SST.

are physically linked (Leuliette and Wahr, 1999; Ciani et al., 2020) and this link can be learned in a machine learning framework. In several studies, using SST leads to major improvements in SSH inverse problems (Archambault et al., 2022; Fablet et al., 2022).

However, learning physical dynamics in a supervised framework requires high-resolution datasets that are not available in a real-world scenario. Therefore a solution is to use an Observing System Simulation Experiment (OSSE), a twin experiment that simulates the satellite interpolation inverse problem (Gaultier et al., 2016). The dataset produced with this method enables us to train a deep neural network in a supervised way, and then perform a transfer learning to real-world data. Nevertheless, we have no guarantee that the simulation is truly realistic.

To overcome the issue raised by the lack of ground truth data, we present in this work a method denoted Multimodal Unsupervised Spatio-Temporal Interpolation (MUSTI) able to train a deep neural network in an operational scenario, i.e. with only the SST images and the SSH along-track measurements. The main idea of this method is to estimate SSH images from SST fully gridded images while supervising the multimodal information transfer only at the location where we have access to measurements. From the cross-modal learning point of view, it can be seen as a Weakly-Supervised task, but from the inpainting point of view, it is an unsupervised problem as we have access to no fully gridded image. We test our method with two different neural architectures and on three datasets (two of them are simulated and one remote-sensed). We show promising results to include information from multimodal sources in im-

age inverse problems and compare MUSTI to the operational product (DUACS), to fully supervised neural networks, and to data assimilation methods.

2 PROBLEM STATEMENT

2.1 Satellite tracks interpolation

Satellite remote sensing involves numerous inverse problems, such as denoising, super-resolution, or interpolation. Among them, gridding altimetry maps is a challenging ocean application combining an interpolation and a denoising image inverse problem. Let us consider a time window of T days with multimodal observations of SSH and SST. We denote hereafter Y_{sst}^t and Y_{ssh}^t respectively the SST and SSH observations at time t and X_{ssh}^t the true SSH state i.e. the gridded image that we aim to recover. Due to the high resolution of the SST observations, we can consider them as gridded images, even in a real-world framework. The SSH observations, on the other hand, can not be considered gridded images as the measurements are sparse.

Formally we consider that SSH tracks are obtained from the true SSH state image X_{ssh}^t using an observation operator $\mathcal{H}_{\Omega_t}$ such as in Eq. (1):

$$Y_{ssh}^t = \mathcal{H}_{\Omega_t}\left(X_{ssh}^t\right) + \varepsilon_t \tag{1}$$

where Ω_t is the support of the SSH observations at time t and ε_t is the observation noise well-detailed by (Gaultier et al., 2016). These two parameters can be simulated using a twin experiment software, but

in the real-world only Ω_t is known where ε_t must be estimated.

To simplify the notations, in the following we refer to the observations on the entire time window as $\mathbf{Y}_{sst} = \{Y_{sst}^1, \ldots, Y_{sst}^T\}$ and same with $\mathbf{Y}_{ssh}$. Eq. (1) is now expressed in a compact way by Eq.(2):

$$\mathbf{Y}_{ssh} = \mathcal{H}_\Omega(\mathbf{X}_{ssh}) + \varepsilon \qquad (2)$$

with $\varepsilon = \{\varepsilon_1, \ldots, \varepsilon_T\}$ and $\Omega = \bigcup_{t=1}^T \Omega_t$.

2.2 Overview of methods

2.2.1 Data assimilation

In geosciences applications, the issue of fitting and validating methods is a challenging task as the ground truth is never accessible. The community thus uses data assimilation schemes combining physical information together with observations to regularize the inversion. A wide range of model-driven methods has been proposed to inverse Eq. (2). For instance, the operational product DUACS (Taburet et al., 2019) relies on a Best Linear Unbiased Estimator (BLUE) method (Bretherton et al., 1976). This linear interpolation requires estimating the covariance matrices of the system state and noise. This statistical information is hard to estimate in a geosciences context; in the case of DUACS method, it involves 25 years of data acquisition and a strong preprocessing physical expertise. DUACS is challenged by other data assimilation methods (Ardhuin et al., 2020; Ballarotta et al., 2020; Le Guillou et al., 2020), combining a physical model of the Ocean with observations. These approaches use Surface Quasi-Geostrophic (SQG) theory (Klein et al., 2009) to constrain the image inverse problem, but also require the knowledge of the covariance matrices.

2.2.2 Supervised machine learning

Machine learning methods, for their part, use statistical information to learn the inversion. Deep learning networks can model complex relationships between multimodal data (Ngiam et al., 2011) and their flexibility makes them suitable to include SST information in the interpolation (Nardelli et al., 2022; Archambault et al., 2022; Fablet et al., 2022). Recently, (Fablet et al., 2021) introduced 4DVarNet, a supervised deep learning network with state-of-the-art performances on simulated data. This method is fitted on a twin experiment and then applied to the real world.

2.2.3 Unsupervised machine learning

Despite supervised schemes, neural network architectures can be used to introduce an inductive bias suited to image inverse problems as in the paper Deep Image Prior (DIP) (Ulyanov et al., 2017). Replacing DUACS BLUE covariance statistics with a Spatio-Temporal deep image prior is already proven efficient to perform the OI of satellite tracks (Filoche et al., 2022). As they do not need to be trained on full fields, these methods can be applied directly to real data.

2.3 Data

In the following, we present two datasets used to test interpolation methods, the NATL60 Observing System Simulation Experiment (OSSE)[1], and a real-world scenario with satellite altimetry along tracks SSH[2] and SST[3].

2.3.1 Observing System Simulation Experiment (OSSE)

To test the reconstruction quality of the different methods we use an Observing System Simulation Experiment. To do so, a high-resolution simulation NATL60 (Ajayi et al., 2019) is considered as ground truth, upon which we simulate satellite orbits and measurements with realistic instrumental noise. It includes SWOT wide swaths, and nadir pointing observations as shown in Figure 1. Both tracks and measurement errors are performed by the swot-simulator software (Gaultier et al., 2016). As shown in Figure 2, the daily data coverage of the observations is about 10% on average with strong periodic variations due to the SWOT satellite's path. Even when the data coverage reaches 20%, important Spatio-Temporal gaps remain (see the second row of Figure 1), hence the difficulty of the interpolation task.

To complete the operational framework we use the SST from NATL60 simulation without noise. This data is thus not a realistic image as clouds and other noise sources should be added to be closer to real temperature observations. However, as we will test our method on real-world data as well, in this first experience we choose not to add any noise to the SST image. Since this high-resolution simulation is very computationally intensive, we only have access to one year of simulation, from the 1st of October 2012 to the 30th of September 2013. The first 21 days are used to spin

---

[1]More information about the OSSE data is provided at https://github.com/ocean-data-challenges/2020a_SSH_mapping_NATL60

[2]Real-world altimetry data are provided at https://github.com/ocean-data-challenges/2021a_SSH_mapping_OSE

[3]MUR SST data are freely available at https://podaac.jpl.nasa.gov/dataset/MUR-JPL-L4-GLOB-v4.1
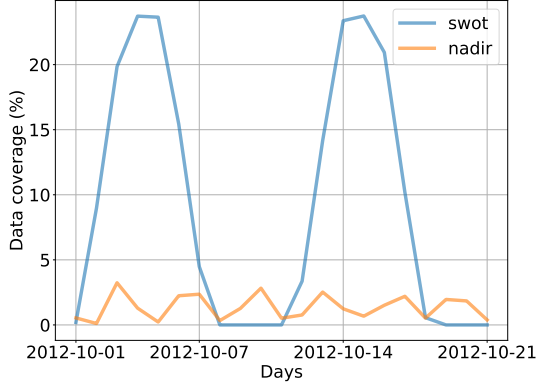
Figure 2: Data coverage on October 2012 with the swot-simulator software on the study area. The SWOT satellite provides more points than the multiple nadir satellites but has a high return time (11 days). Combined, the SWOT and nadir altimeters cover each day 10.5% of the studied area on average.

up the methods that need it, then 42 days of simulation are used as a test set. To avoid data leakage between the test and the training data, we set aside 31 intermediary days of simulation and take the rest as a training set.

We focus on a part of the North Atlantic Ocean: the Gulf Stream area, from latitude 33° to 43° and from longitude -65° to -55°. This area is very energetic, with strong currents, so we expect a significant synergy between SSH and SST. Also for computational purposes, we re-grid all images at a resolution of 0.05° in latitude and longitude (where the NATL60 simulation has a resolution of 0.01°).

2.3.2 Real-World data

The OSSE data provide an idealistic scenario, with an optimal combination of altimeters and a noiseless sea surface temperature. Thus the surface temperature and height are overly correlated compared to a realistic scenario and the multimodal link between data should be easy to learn by a neural network. This motivates us to test the same method on real-world data. We use measures from different nadir altimeters acquired between the 1st of December 2017 to the 31st of January 2018. Once again to evaluate the method we leave aside the altimeter data from Cryosat-2 as a test set and some observations of another satellite (Jason 2) as a validation set. We underline the fact that as the SWOT mission is not launched yet, no data with wide swaths is available today.

We use temperature data from the Multi-scale Ultra-high Resolution (MUR) SST (Chin et al., 2017). These SST satellite images are an operational delayed time product available with only a 4-day latency.

3 PROPOSED METHOD

3.1 From supervised to unsupervised inversion

Data assimilation and machine learning methods leverage different ways to constrain the inversion with different drawbacks. For instance, the models needed by data assimilation methods can be computationally intensive and suffer from various sources of error due to discretization or unresolved physics among others (Janjić et al., 2018). Also, some of the assimilation methods require the adjoint model which is not always available. On the other hand, the supervised machine learning frameworks need ground truth and thus use output data of complex physical models. If 4DVarNet has proven its capacity to interpolate the simulated data, transposing this training to real-world scenarios is still challenging and leads to domain adaptation issues. The performance of this approach does not only rely on the ability of a neural network to learn the physics embedded in the model but also on the trust that we have in the NATL60 simulation itself.

Taking into account these elements, we propose a method, named MUSTI, to train a deep learning network in an operational scenario without using simulations. To that end, we rely on two main features; the prior induced by the neural network and the statistical link between the multimodal observations. Our method differs from 4DVarNet for it is not supervised on ground truth and from Deep Image Prior as it can include multimodal observations and is fitted on a dataset.

3.2 Multimodal Unsupervised Spatio-Temporal Interpolation

As suggested by the manifold hypothesis (Fefferman et al., 2016), physical data can be seen as high-dimension observations taken from the same underlying representation. This means that the ocean system can be parsimoniously described using a low-dimension representation vector denoted $\mathbf{Z}$ able to encode its core dynamics.

Considering the above arguments, using an encoder-decoder framework seems appropriate. One can use a deep neural network to encode $\mathbf{Y}_{sst}$ in the latent space by modeling $p(\mathbf{Z}|\mathbf{Y}_{sst})$. A decoder can then recover the output distribution $p(\mathbf{X}_{ssh}|\mathbf{Z})$ and transfer information from the SST gridded image to a SSH image. Hereafter the encoder will be denoted f_{θ_1} in Eq. (3), the decoder g_{θ_2} in Eq. (4) and the encoder-decoder network $h_\theta = g_{\theta_2} \circ f_{\theta_1}$. Other architectures
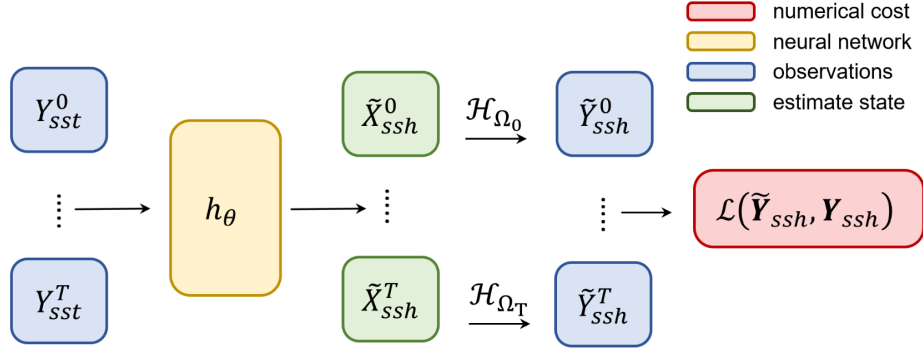
Figure 3: Computation graph of the proposed method. The neural network h_θ holds all the control parameters θ and aims to generate a time series of SSH images from a time series of SST images. This method can use any kind of neural network architecture for h_θ, as long as it takes an image time series as input and output. The masking operator $\mathcal{H}_\Omega$ is applied before the cost function in order to train the network in an unsupervised manner.

can be used as well through a direct multimodal information transfer from $\mathbf{Y}_{sst}$ to $\mathbf{X}_{ssh}$ as long as they bring an inductive bias, helping the reconstruction.

$$\text{Encoding:} \qquad \tilde{\mathbf{Z}} = f_{\theta_1}\left(\mathbf{Y}_{sst}\right) \qquad (3)$$

$$\text{Decoding:} \qquad \tilde{\mathbf{X}}_{ssh} = g_{\theta_2}\left(\tilde{\mathbf{Z}}\right) \qquad (4)$$

$$\text{Masking:} \qquad \tilde{\mathbf{Y}}_{ssh} = \mathcal{H}_\Omega\left(\tilde{\mathbf{X}}_{ssh}\right) \qquad (5)$$

The MUSTI method consists in encoding the SST observations as in Eq. (3) as a latent vector $\tilde{\mathbf{Z}}$. Then following Eq. (4) the SSH gridded state $\tilde{\mathbf{X}}_{ssh}$ is estimated from the latent space. Finally, as we want the neural network to be trained in an unsupervised way, we apply the masking operator $\mathcal{H}_\Omega$ to the estimate SSH state $\tilde{\mathbf{X}}_{ssh}$ to retrieve along-tracks observations $\tilde{\mathbf{Y}}_{ssh}$ as Eq. (4) suggests.

By doing so, we can supervise the network only on the pixels where we have access to observations. This means that, similarly to Deep Image Prior inpainting scheme (Ulyanov et al., 2017), we compute a supervised loss $\mathcal{L}$ between $\tilde{\mathbf{Y}}_{ssh}$ and $\mathbf{Y}_{ssh}$, Eq. (6).

$$\mathcal{L}\left(\tilde{\mathbf{Y}}_{ssh}, \mathbf{Y}_{ssh}\right) = \sum_{t=0}^{T}\left\|\tilde{Y}_{ssh}^t - Y_{ssh}^t\right\|^2$$
$$= \sum_{t=0}^{T}\left\|\mathcal{H}_{\Omega_t}\left(\tilde{X}_{ssh}^t\right) - Y_{ssh}^t\right\|^2 \qquad (6)$$

The MUSTI method aims in learning a multimodal physical link between the gridded SST and the along-track SSH. The implicit hypothesis behind our method is that fitting a neural architecture to model $p\left(\mathbf{Y}_{ssh}|\mathbf{Y}_{sst}\right)$ will provide a good estimation of the true state $\mathbf{X}_{ssh}$ even on the pixels where it is not supervised to do so. We believe that due to the symmetry by translation of the convolution operation, the fea-

tures learned on along tracks measurements will apply the same physical transformation to every pixel of the SST image to generate the gridded SSH map. We present a visual overview of this method in Figure 3.

4 RESULTS

4.1 Experiment

The MUSTI training procedure can be used with a wide range of convolutional neural architectures as long they bring an inductive bias toward out of tracks generalization. We test two deep neural network architectures following the MUSTI method: a U-net architecture (Ronneberger et al., 2015) and a Spatio-Temporal auto-encoder (STAE). It relies on the Spatio-Temporal convolution (conv2DP1) introduced by (Tran et al., 2018). More details about the STAE architecture are provided in Appendix B. Previous work has shown that this kind of convolution introduces a Spatio-Temporal prior well suited for satellite track interpolation in an unlearned framework (Filoche et al., 2022). Using a network architecture relying on the same principles, we use conv2DP1 and 3D maxpooling to reduce the time series spatial dimension while preserving time encoding.

Thus we can compare the performance of a network compressing information in a latent space and the performance of a direct network. Hereafter we will discuss 3 different scenarios: the OSSE data with SWOT and nadir measures, with only nadir measures, and the real-world data.

Table 1: Results of the different methods on the three data scenarios. We present hereafter the score of the different interpolation methods to which we compare ourselves. We give the score of the MUSTI method for an ensemble of 10 neural networks with different weights initialization and the mean performance of each member of the ensemble. The details about the tuned hyper-parameters are given in Appendix A

Methods	swot + nadir				nadir only				real-world data	
	μ	σ_t	λ_x	λ_t	μ	σ_t	λ_x	λ_t	μ	σ_t
DUACS	0.922	0.017	1.22	11.29	0.916	0.008	1.42	12.08	0.877	0.065
DYMOST	0.926	0.018	1.19	10.26	0.911	0.013	1.35	11.87	0.889	**0.064**
MIOST	0.938	0.012	1.18	10.33	0.927	0.007	1.34	10.34	0.887	0.085
BFN	0.926	0.018	1.02	10.37	0.919	0.017	1.23	10.64	0.879	0.065
4DVarNet*	**0.959**	**0.009**	**0.62**	4.31	0.944	**0.006**	**0.84**	7.95	0.889	0.089
MUSTI U-net mean	0.951	0.01	1.09	6.0	0.939	0.009	1.35	5.73	0.881	0.103
MUSTI U-net ensemble	0.954	**0.009**	**0.62**	**3.44**	**0.946**	0.008	1.23	**4.14**	0.886	0.099
MUSTI STAE mean	0.945	0.011	1.02	6.32	0.931	0.012	1.13	8.78	0.885	0.086
MUSTI STAE ensemble	0.952	0.011	0.68	5.41	0.938	0.012	0.96	7.59	**0.893**	0.083

* supervised

4.1.1 Training procedure

For each scenario and neural architecture we tune the window size T, and the stopping epoch on the validation dataset, as described in Appendix C. FLAG In the real-world scenario, there is no ground truth to serve as a validation dataset, therefore we leave aside the observations from a satellite (Jason-2g) to tune the model's hyper-parameters on. Once these hyper-parameters are found on validation observations, we train another network with this set of parameters on the training and validation set. This way we can fully compare to other methods in terms of used altimetry observations.

As the optimization path varies with weight initialization, we train a set of 10 models for each experience and average generated images from each model. This ensemble of neural networks helps to stabilize performances regarding to initialization and is proven to enhance the reconstruction (Filoche et al., 2022; Hinton and Dean, 2015).

4.1.2 Method evaluation

To compare the reconstruction methods we use the metrics defined by (Le Guillou et al., 2020) including the normalized root mean squared (*NRMSE*) as in Eq. (7):

$$NRMSE\,(t, \mathbf{y}, \tilde{\mathbf{y}}) = 1 - \frac{RMSE\,(\mathbf{y}^t, \tilde{\mathbf{y}}^t)}{RMS\,(\mathbf{y})} \qquad (7)$$

with Root Mean Squared Error as *RMSE* and with Root Mean Squared of the target **y** during the entire evaluation time domain as *RMS*(**y**). We call in Table 1 μ the mean of the *NRMSE* on the time domain and σ_t its time standard deviation. These metrics have no units and for a perfect reconstruction μ equals 1.

We also use two spectral metrics, λ_x (in degrees) and λ_t (in days) that can be assimilated respectively to the minimum spatial and temporal wavelength resolved. We do not compute these spectral metrics for the real-world scenario, because we do not have a gridded ground truth. For more details about the implementation of these metrics, we refer the reader to (Le Guillou et al., 2020). All metrics given in Table 1 are computed on the image at the center of the time series.

4.2 Comparison of the methods on OSSE and real-world data

We compare the results of different methods: the operational linear interpolation using a covariance matrix tuned with 25 years of observations (DUACS), three model-based data assimilation schemes: DYMOST (Ubelmann et al., 2016; Ballarotta et al., 2020), MIOST (Ardhuin et al., 2020) and BFN (Le Guillou et al., 2020). Finally, we compare with the supervised neural network 4DVarNet (Fablet et al., 2021).

- In the **swot + nadir** scenario 4DVarNet outperforms other methods in terms of RMSE, especially DUACS and the model-driven approaches. The MUSTI method can not compare with the supervised scheme RMSE-wise but has similar results in terms of minimum spatial and temporal wavelength resolved. The U-net architecture gives better results than STAE. In Figure 4 we present a visual comparison of the DUACS method and a MUSTI U-net. We see that the DUACS method misses some of the small-scale variations that the MUSTI method is able to resolve.

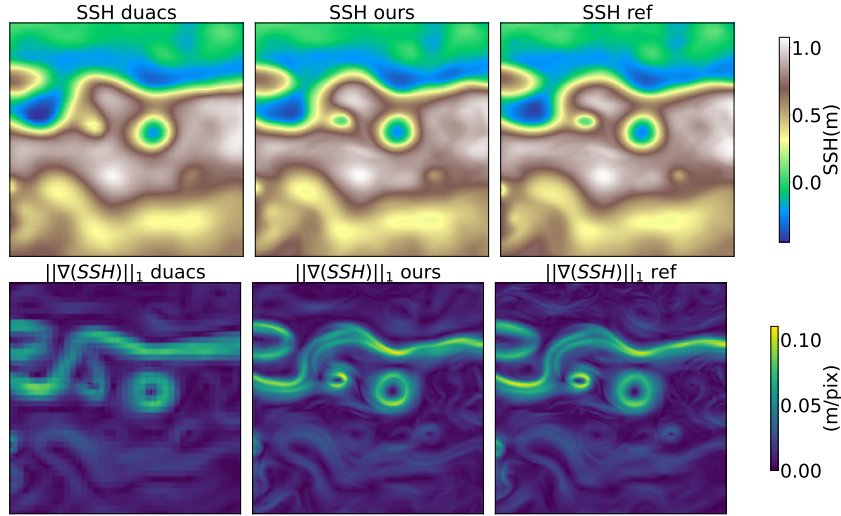- In the **nadir only** scenario, no wide swath altime-

Figure 4: Visual overview of the visual results in the swot+nadir scenario. We compare DUACS and an U-net trained following the MUSTI method. We present the generated SSH image and the norm of the gradient.

try data are available, thus the performances of all unsupervised methods drop by approximately 0.01 in terms of normalized RMSE. But the supervised neural network has a higher performance drop, so in the end, the U-net trained in a MUSTI way has a slightly better RMSE and temporal resolution. However, we notice a significant drop in the reconstruction of the short spatial wavelength. This can be explained by the fact that lacking large satellite swath, the small eddies are missed.

- On the **real-world data**, every method has a very significant RMSE performance drop. The DYMOST, MIOST, and 4DVarNet methods are in a nutshell, while DUACS and BFN are outperformed. Surprisingly, the two networks trained with MUSTI method do not have the same order of performance as on the OSSE data. The STAE ensemble outperforms other methods, while the U-net does not reach DYMOST, MIOST and 4DVarNet. It seems that the encoding-decoding process is useful to denoise the SST images while a skip connection is not able to do so.

These results demonstrate the potential of unsupervised neural networks to deal with partially observed fields. The MUSTI method that was designed for an operational framework achieves better results in the real-world scenario, directly learning from real-world fields than a method supervised on an independent dataset. Furthermore, we show that it is possible to transfer multimodal information from the SST to the SSH fields without providing any covariance matrix, physical model information, or supervision with a full-field dataset.

5 PERSPECTIVES

In the following, we discuss different ways to continue this work.

Using MUSTI method in a transfer learning scheme Our method allows us to train a neural network with incomplete data as an operational framework requires. However, this method could also be used in a transfer learning scheme. We are interested in training a deep learning architecture on OSSE data in a traditional supervised way, and then using MUSTI method to fine-tune the model on real-world data.

Multimodal fusion There are different ways to perform multimodal data fusion (Ngiam et al., 2011) and we are interested in testing other fusion approaches. For instance, if this training procedure is capable to fit a trajectory of SST to a trajectory of SSH it does not generalize well to new examples. Being able to give SSH ground tracks as inputs of the network without overfitting them should help solve this problem.

6 CONCLUSION

We presented a method to include multimodal information in Spatio-Temporal image inverse problems in an unsupervised way. Relying on the hidden physical link between Sea Surface Height and Sea Surface Temperature, we train a neural network to fit the SSH along tracks observations starting from a fully gridded SST image. We show that the multimodal trans-

fer performed by the network on the along-tracks data generalizes well where it has not been supervised. We tested two different neural architectures, a U-net and a Spatio-Temporal auto-encoder, on 3 datasets (2 simulations and a real-world scenario).

On real-world data, we report a relative improvement of 13% compared to the operational product (DUACS) in terms of RMSE. We also show that our method is able to outperform supervised state-of-the-art interpolation architectures as they suffer from overfitting of the simulation upon which they are trained.

REFERENCES

Ajayi, A., Le Sommer, J., Chassignet, E., Molines, J.-M., Xu, X., Albert, A., and Cosme, E. (2019). Spatial and temporal variability of north atlantic eddy field at scale less than 100 km. *Earth and Space Science Open Archive*, page 28.

Amores, A., Jordà, G., Arsouze, T., and Le Sommer, J. (2018). Up to what extent can we characterize ocean eddies using present-day gridded altimetric products? *Journal of Geophysical Research: Oceans*, 123:7220–7236.

Archambault, T., Charantonnis, A., Béréziat, D., and Thiria, S. (2022). SSH Super-Resolution using high resolution SST with a Subpixel Convolutional Residual Network. In *Climate Informatics*.

Ardhuin, F., Ubelmann, C., Dibarboure, G., Gaultier, L., Ponte, A., Ballarotta, M., and Faugère, Y. (2020). Reconstructing ocean surface current combining altimetry and future spaceborne doppler data. Earth and Space Science Open Archive.

Ballarotta, M., Ubelmann, C., Rogé, M., Fournier, F., Faugère, Y., Dibarboure, G., Morrow, R., and Picot, N. (2020). Dynamic mapping of along-track ocean altimetry: Performance from real observations. *Journal of Atmospheric and Oceanic Technology*, 37:1593–1601.

Bretherton, F., Davis, R., and Fandry, C. (1976). A technique for objective analysis and design of oceanographic experiments applied to MODE-73. *Deep-Sea Research and Oceanographic Abstracts*, 23:559–582.

Chin, T. M., Vazquez-Cuervo, J., and Armstrong, E. M. (2017). A multi-scale high-resolution analysis of global sea surface temperature. *Remote Sensing of Environment*, 200:154–169.

Ciani, D., Rio, M.-H., Bruno Nardelli, B., Etienne, H., and Santoleri, R. (2020). Improving the altimeter-derived surface currents using sea surface temperature (SST) data: A sensitivity study to SST products. *Remote Sensing*, 12:1601.

Emery, W. J., Brown, J., and Nowak, Z. P. (1989). AVHRR image navigation-summary and review. *Photogrammetric engineering and remote sensing*, 4:1175–1183.

Fablet, R., Amar, M., Febvre, Q., Beauchamp, M., and Chapron, B. (2021). End-to-end physics-informed representation learning for satellite ocean remote sensing data: Applications to satellite altimetry and sea surface currents. *ISPRS Annals of the Photogrammetry, Remote Sensing and Spatial Information Sciences*, 5:295–302.

Fablet, R., Febvre, Q., and Chapron, B. (2022). Multimodal 4DVarNets for the reconstruction of sea surface dynamics from sst-ssh synergies. ArXiv.

Fefferman, C., Mitter, S., and Narayanan, H. (2016). Testing the manifold hypothesis. *Journal of the American Mathematical Society*, 29:983–1049.

Filoche, A., Archambault, T., Charantonis, A., and Béréziat, D. (2022). Statistics-free interpolation of ocean observations with deep spatio-temporal prior. In *ECML/PKDD Workshop on Machine Learning for Earth Observation and Prediction (MACLEAN)*.

Gaultier, L., Ubelmann, C., and Fu, L. (2016). The challenge of using future SWOT data for oceanic field reconstruction. *Journal of Atmospheric and Oceanic Technology*, 33:119–126.

Hinton, G. and Dean, J. (2015). Distilling the knowledge in a neural network. In *NIPS Deep Learning and Representation Learning Workshop*.

Jam, J., Kendrick, C., Walker, K., Drouard, V., Hsu, J., and Yap, M. (2021). A comprehensive review of past and present image inpainting methods. *Computer Vision and Image Understanding*, 203.

Janjić, T., Bormann, N., Bocquet, M., Carton, J. A., Cohn, S. E., Dance, S. L., Losa, S. N., Nichols, N. K., Potthast, R., Waller, J. A., and Weston, P. (2018). On the representation error in data assimilation. *Quarterly Journal of the Royal Meteorological Society*, 144(713):1257–1278.

Klein, P., Isem-Fontanet, J., Lapeyre, G., Roullet, G., Danioux, E., Chapron, B., Le Gentil, S., and Sasaki, H. (2009). Diagnosis of vertical velocities in the upper ocean from high resolution sea surface height. *Geophysical Research Letters*, 36.

Le Guillou, F., Metref, S., Cosme, E., Ubelmann, C., Ballarotta, M., Verron, J., and Le Sommer, J. (2020). Mapping altimetry in the forthcoming SWOT era by back-and-forth nudging a one-layer quasi-geostrophic model. Earth and Space Science Open Archive.

Leuliette, E. W. and Wahr, J. M. (1999). Coupled pattern analysis of sea surface temperature and TOPEX/Poseidon sea surface height. *Journal of Physical Oceanography*, 29(4):599–611.

McCann, M., Jin, K., and Unser, M. (2017). Convolutional neural networks for inverse problems in imaging: A review. *IEEE Signal Processing Magazine*, 34:85–95.

Nardelli, B., Cavaliere, D., Charles, E., and Ciani, D. (2022). Super-resolving ocean dynamics from space with computer vision algorithms. *Remote Sensing*, 14:1159.

Ngiam, J., Khosla, A., Kim, M., Nam, J., Lee, H., and Ng, A. Y. (2011). Multimodal deep learning. In *Proceedings of the 28th International Conference on Interna-*

tional Conference on Machine Learning, ICML 11, page 689–696, Madison, WI, USA. Omnipress.

Ongie, O., Jalal, A., Metzler, C., Baraniuk, R., Dimakis, A., and Willett, R. (2020). Deep learning techniques for inverse problems in imaging. *IEEE Journal on Selected Areas in Information Theory*, 1:39–56.

Qin, Z., Zeng, Q., Zong, Y., and Xu, F. (2021). Image in-painting based on deep learning: A review. *Displays*, 69:102028.

Ronneberger, O., Fischer, P., and Brox, T. (2015). U-net: Convolutional networks for biomedical image segmentation. In *MICAI*, pages 234–24.

Stegner, A., Le Vu, B., Dumas, F., Ghannami, M., Nicolle, A., Durand, C., and Faugere, Y. (2021). Cyclone-anticyclone asymmetry of eddy detection on gridded altimetry product in the mediterranean sea. *Journal of Geophysical Research: Oceans*, 126.

Taburet, G., Sanchez-Roman, A., Ballarotta, M., Pujol, M.-I., Legeais, J.-F., Fournier, F., Faugere, Y., and Dibarboure, G. (2019). DUACS DT2018: 25 years of reprocessed sea level altimetry products. *Ocean Sci*, 15:1207–1224.

Tran, D., Wang, H., Torresani, L., Ray, J., Lecun, Y., and Paluri, M. (2018). A closer look at spatiotemporal convolutions for action recognition. *Proceedings of the IEEE Computer Society Conference on Computer Vision and Pattern Recognition*, pages 6450–6459.

Ubelmann, C., Cornuelle, B., and Fu, L. (2016). Dynamic mapping of along-track ocean altimetry: Method and performance from observing system simulation experiments. *Journal of Atmospheric and Oceanic Technology*, 33:1691–1699.

Ulyanov, D., Vedaldi, A., and Lempitsky, V. (2017). Deep image prior. *International Journal of Computer Vision*, 128:1867–1888.

Wang, Z., Chen, J., and Hoi, S. (2021). Deep learning for image super-resolution: A survey. *IEEE Transactions on Pattern Analysis and Machine Intelligence*, pages 3365–3387.

A   Implementation details

All networks are trained through an ADAM optimizer with the following parameters: $\beta_1 = 0.9$, $\beta_2 = 0.999$. We use an exponential learning rate scheduler with a starting learning rate of 10^{-3} for the U-net and of 5×10^{-4} for the STAE and $\alpha = 0.96$.

We determine the optimal hyper-parameters (window temporal size T and stopping epoch) on the validation dataset, other hyper-parameters are untuned.

Table 2: Optimal hyper-parameters on the validation dataset for each architecture and dataset.

Dataset	STAE		U-net	
	T	epoch	T	epoch
s+n	7	94	3	113
n	5	57	5	60
rw	5	50	5	55

B   Network architectures [4]

Spatio-Temporal Auto-Encoder

The architecture of the Spatio-Temporal Auto-Encoder (STAE) is given in our code and relies on the Conv2PD1 introduced by (Tran et al., 2018). First, a 2D convolution is performed in the spatial dimensions, then a 3D Batch-Normalization followed by a ReLU activation function and finally a 1D convolution in the time dimension. The spatial dimensions of the image are then divided by 2 (the time dimension is not reduced) with a 3D max pooling.

The decoder is similar to the encoder except that we use a 3D upsampling (trilinear) and then a Conv2DP1. The last block has no Batch-Normalization nor ReLU activation function.

U-net

The U-net (Ronneberger et al., 2015) architecture is a classic image architecture. We use four downward blocks composed of two 2D convolutions, each one with a ReLU activation function and BatchNormalization. A Maxpooling is then performed to divide the size of the image by two.

C   Train, validation, test split

Table 3: Train, validation, and test datasets for each scenario

Dataset	OSSE	Real-world
Train	Tracks from all year	every nadir satellite except **j2g** and **c2**
Validation	GT between **2013-01-02** and **2013-09-30**	nadir tracks from **j2g** satellite
Test	GT between **2012-10-22** and **2012-12-02**	nadir tracks from **c2** satellite

---

[4]our code is available at https://gitlab.lip6.fr/archambault/visapp2023